Acta Metall. Sin. (Engl. Lett.), 2014, **27**(4), 723–729
DOI 10.1007/s40195-014-0109-4

Microstructure and Strain Hardening of a Friction Stir Welded High-Strength Al–Zn–Mg Alloy

A. H. Feng · D. L. Chen · Z. Y. Ma · W. Y. Ma · R. J. Song

Received: 24 November 2013 / Revised: 20 February 2014 / Published online: 30 July 2014

Abstract Microstructural evolution and strain hardening behavior of a friction stir welded (FSWed) high-strength 7075Al-T651 alloy were evaluated. The nugget zone was observed to consist of fine and equiaxed recrystallized grains with a low dislocation density and free of original precipitates, but containing uniformly distributed dispersoids. The strength, joint efficiency, and ductility of the FSWed joints increased with increasing welding speed. A joint efficiency of ~91% was achieved at a welding speed of 400 mm/min and rotational rate of 800 r/min, while the ductility remained basically the same as that of the base metal. There was no obvious strain rate sensitivity observed in both base metal and welded joints. While both the base metal and FSWed joints exhibited stage III and IV hardening characteristics, the hardening capacity, strain hardening exponent, and strain hardening rate all increased after friction stir welding.

KEY WORDS: Aluminum alloy; Friction stir welding; Mechanical properties; Strain hardening

1 Introduction

7xxx series aluminum alloys are precipitation hardened Al–Zn–Mg–(Cu) alloys, which have been used extensively in the aircraft structural components, moving equipment, and other highly stressed load-bearing applications [1]. The structural applications of aluminum alloys unavoidably involve welding and joining, which are fairly challenging using conventional fusion welding processes. Friction stir welding (FSW), developed by The welding institute (TWI) of UK [2], provides a promising solution, since it is an energy-effective and environment-friendly solid-state joining technique that offers significant advantages over conventional joining processes due to the absence of fusion zone [3–6]. FSW is an enabling technique especially capable of welding light-weight alloys, e.g., aluminum alloys [2–5], magnesium alloys [7–12], and titanium alloys [13, 14]. Numerous studies have thus been conducted to optimize the welding process parameters, such as the effects of welding speed, rotational rate, welding tool geometry, etc., which have been well documented [3–5]. Extensive studies on the FSW/FSP of

Available online at http://link.springer.com/journal/40195

A. H. Feng · R. J. Song
School of Materials Science and Engineering, Tongji University, Shanghai 200092, China
e-mail: aihanfeng@tongji.edu.cn

A. H. Feng · W. Y. Ma
State Key Laboratory of Advanced Welding Production Technology, School of Materials Science and Engineering, Harbin Institute of Technology, Harbin 150001, China

D. L. Chen (✉)
Department of Mechanical and Industrial Engineering, Ryerson University, Toronto, ON M5B 2K3, Canada
e-mail: dchen@ryerson.ca

Z. Y. Ma
Shenyang National Laboratory for Materials Science, Institute of Metal Research, Chinese Academy of Sciences, Shenyang 110016, China

7xxx series aluminum alloys have also been reported including the microstructure evolution [15–19] and the mechanical properties [20–22]. However, only limited studies have been reported on the strain hardening of FSW/FSPed lightweight alloys [8, 12, 23–26], although strain hardening behavior is one of the important considerations in the evolution of plastic deformation of materials. The strain hardening capacity is intimately related to the deformability, ductility, and toughness of materials. Afrin et al. [8], Chowdhury et al. [12], and Lin and Chen [24] reported the strain hardening behavior of FSWed magnesium alloys, while Hu et al. [23] presented the strain hardening rate of a FSPed Al–Zn alloy, Xu et al. [25] evaluated the strain hardening behavior of a FSWed AA2219 Al alloy, and Simar et al. [26] studied flow and strain hardening behavior of various zones of a FSWed 6005A-T6 aluminum alloy using micro-tensile specimens cut parallel to the welding direction. Also, Khodaverdizadeh et al. [27] studied the influence of FSW parameters on strain hardening behavior of pure copper joints. To the authors' knowledge, no studies on the strain hardening of FSWed 7075Al alloy have been reported in the literature. It is unclear how the welding parameter affects the strain hardening behavior and if the FSWed 7075 Al joint exhibits strain rate sensitivity. The objective of the present study was, therefore, to examine the microstructural evolution and strain hardening behavior of a FSWed 7075Al-T651 alloy, and we attempt to examine the difference of strain hardening behavior between the unwelded base metal and FSWed joints based on the Kocks–Mecking analysis.

2 Experimental

6.35-mm-thick 7075Al-T651 rolled plates (400 mm long and 100 mm wide), with a composition of 5.6Zn-2.5 Mg-0.5Fe-0.16Cu-0.23Cr-0.3Mn-0.2Ti (wt%), were FSWed along the rolling direction using a FSW machine. A steel tool with a shoulder of Φ20 mm and a cylindrical threaded pin of Φ8 mm was used. The tool rotational rate was selected to be 800 r/min with a varying welding speed from 100 to 400 mm/min.

Microstructural characterization was carried out using light microscope, scanning electron microscope (SEM) equipped with Oxford energy-dispersive X-ray spectroscopy (EDS), and transmission electron microscope (TEM). TEM foils were prepared by twin-jet electropolishing using a solution of 70% methanol and 30% nitric at −35 °C and 19 V. Sub-sized tensile specimens following ASTM E8 standards, with a gage section of 25 mm × 6 mm × 5.6 mm, were machined perpendicular to the FSW direction. The gage area of the specimens was ground with SiC papers up to a grit number of 1,000 along the loading axis to remove the cutting marks and attain a smooth surface. Tensile tests were carried out using a computerized tensile testing machine at varying strain rates from 1×10^{-5} to 1×10^{-2} s^{-1}. At least two samples were tested at each strain rate. A macroscopic image of the tensile sample showing the failure location was observed in the similar way with our previous paper [22]. The fracture surfaces of the base metal (BM) and FSWed joints were examined using SEM/EDS.

3 Results and Discussion

Figure 1 shows the microstructure of the nugget zone (NZ) in the FSWed 7075Al-T651 joints welded at a rotational rate of 800 r/min at welding speeds of 100 and 400 mm/min, respectively. It is seen that the NZ was characterized by fine and equiaxed recrystallized grain structures. A considerable amount of the dispersoids was randomly distributed, which were determined to be chromium-rich dispersion E phase ($Mg_3Cr_2Al_{18}$), as reported in our previous work by X-ray diffractometry (XRD) and scanning transmission electron microscopy (STEM) coupled with energy-dispersive X-ray spectroscopy (EDS) analysis [22]. No other fine precipitates were observed via TEM examinations at a higher magnification (Fig. 1c, d). The dissolution of the original precipitates was due to the high temperature generated during FSW. The average grain size obtained at a higher welding speed of 400 mm/min (Fig. 1a) was smaller than that obtained at a lower welding speed of 100 mm/min (Fig. 1b) at a given rotational rate of 800 r/min. This was due to the less heat input at a higher welding speed while keeping a constant tool rotational rate. Our previous study indicated that the average grain size decreased from 6.7–4.6 μm with increasing welding speed from 100–400 mm/min [22]. Considering the significant effects of the welding speed and tool rotational rate on the thermal input, Commin et al. [28] and Patel et al. [29] tried to establish relationship between the processing parameter and resulting grain size using the Zener-Hollomon (Z) parameter.

Restoration of aluminum alloys by dynamic recovery (DRV) and dynamic recrystallization (DRX) has been well reviewed [30]. The recrystallization was a nucleation and growth process. The growth was accomplished by the migration of the high angle grain boundaries (HAGBs) [31]. The proposed recrystallization mechanisms during FSW included continuous DRX [16], geometric DRX [32], and discontinuous DRX [32, 33]. The final grain size was generally dominated by the ratio of nucleation rate to the growth rate of new grains [34]. In the NZ of FSWed 7050 Al alloy, the grain sizes of as small as 25–100 nm were observed after tool extraction, and subsequent static annealing resulted in a grain size of 2–5 μm [17]. The NZ normally exhibited fine grains with predominantly HAGBs and a low dislocation density [3]. However, a higher

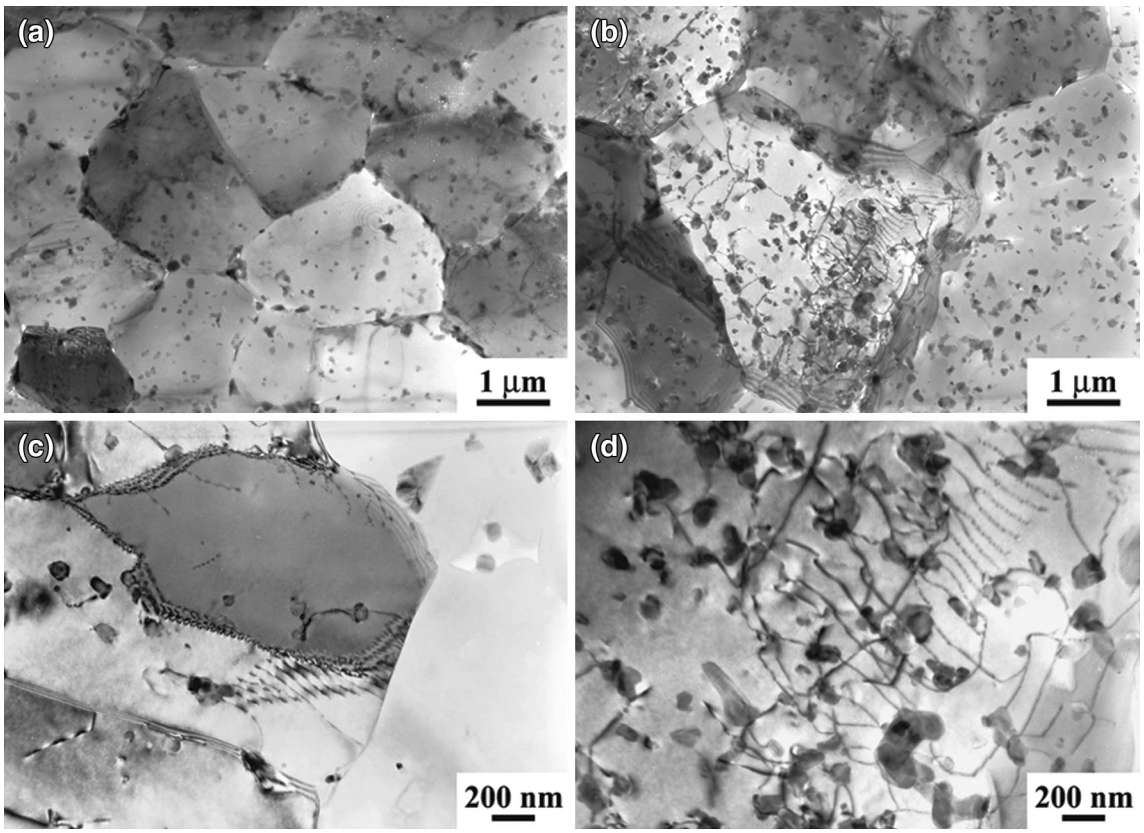

Fig. 1 TEM images of FSWed 7075Al-T651 joints: **a**, **c** 800 r/min and 400 mm/min, **b**, **d** 800 r/min and 100 mm/min

dislocation density in the NZ was observed in 7050-T7451 alloy [16, 20], while a lower dislocation density was reported in 7075Al-T6 alloy [15]. As shown in Fig. 1, the dislocation density in the NZ was indeed quite low. The dislocations piled up against the dispersoid and were absorbed by the subgrain boundaries (Fig. 1c). Such a pinning effect by the dispersoids was also observed in FSWed A6056 alloy [35] and 6061-T651 alloy [36]. The dislocation pile-up near the grain boundary was also observed (Fig. 1d). Rhodes et al. [17] proposed that the final equiaxed grains in their 7050 alloy were formed by grain growth from much finer grains nucleated by the DRX process, thus accounting for the lower dislocation density. It is also likely that, before recrystallization, extensive recovery occurred, as there would be significant plastic flow in the material during FSW [37].

Figure 2 shows the tensile properties of FSWed 7075Al-T651 joints. The BM had a yield strength (YS) of 510 MPa, an ultimate tensile strength (UTS) of 583 MPa and elongation (%El) of 15.4%. At a rotational rate of 800 r/min, YS, UTS, and %El increased with increasing welding speed from 100 to 400 mm/min (Fig. 2a, b). The results were also in agreement with those reported by Mahoney et al. [21]. This was mainly attributed to the smaller grain sizes at a higher welding speed (Fig. 1a, b). As shown in Table 1, the joint efficiency, defined as a ratio of the UTS of welded joints to that of BM, increased with increasing welding speed from ~77% at a welding speed of 100 mm/min to ~91% at a welding speed of 400 mm/min.

The flow stress of a material in the uniform plastic deformation region was commonly expressed by the following Hollomon relationship [37],

$$\sigma = K\varepsilon^n, \tag{1}$$

where n is the strain hardening exponent, K is the strength coefficient, σ is the true stress, and ε is the true strain. Chen and Lu [38] fitted their tensile curves using Ludwik equation,

$$\sigma = \sigma_y + K_1\varepsilon^{n1}, \tag{2}$$

where n_1 is the strain hardening exponent and K_1 is the strength coefficient which represents the increment in strength due to the strain hardening at $\varepsilon = 1$. Equation (1) has been widely used to evaluate the strain hardening exponent. However, the entire true stress–strain curve encompassing the linear elastic deformation stage was imposed to meet Eq. (1), even though only the data between YS and UTS were used in the curve fitting. The following modified equation was then proposed by Afrin et al. [8],

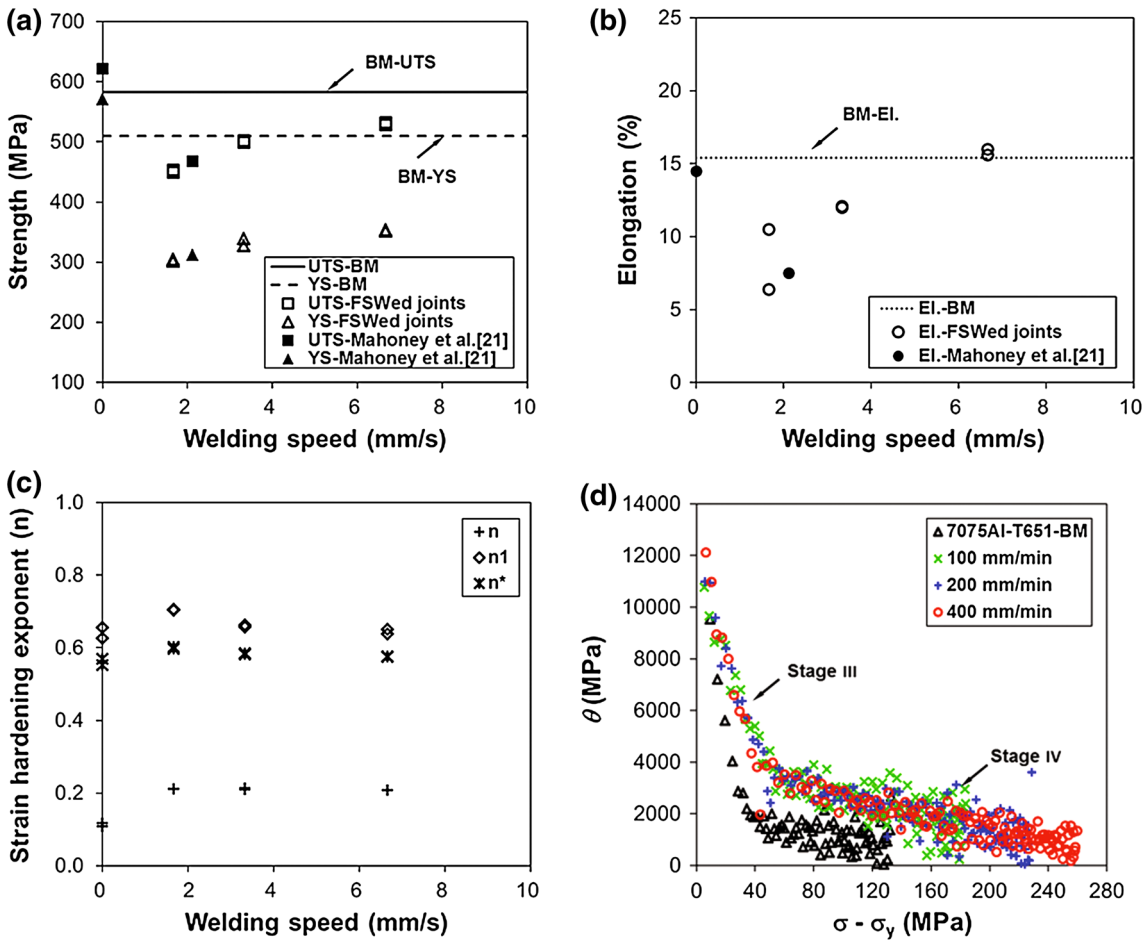

Fig. 2 **a** YS and UTS, **b** ductility, **c** strain hardening exponents versus. welding speed, **d** strain hardening rate (θ) vs. net flow stress ($\sigma - \sigma_y$) for the BM and FSWed joints tested at a strain rate of 1×10^{-3} s^{-1}

Table 1 Summary of joint efficiency and hardening capacity for the 7075Al-T651 alloy tested at a strain rate of 1×10^{-3} s^{-1}

Material	Rotational rate ω (r/min)	Welding speed V (mm/min)	Joint efficiency (%)	Hardening capacity H_c
7075Al-T651 BM	–	–	–	0.14
FSWed 7075Al-T651 joint	800	100	77.1	0.49
			77.8	0.49
	800	200	85.6	0.52
			86.1	0.48
	800	400	90.5	0.50
			91.2	0.50

$$\sigma = \sigma_y + K^*(\varepsilon - \varepsilon_y)^{n*}, \tag{3}$$

where n^*, σ, ε, σ_y, and ε_y are the strain hardening exponent, true stress, true strain, yield strength, and yield strain of a material, respectively. The strain hardening exponents evaluated using Eqs. (1)–(3), were shown in Fig. 2c. It is seen that n^* lay in-between n and n_1, and n was smaller than n_1 and n^*. The FSWed joints showed higher strain hardening exponents compared with the BM. However, the welding speed did not have a strong effect on the strain hardening (Fig. 2c). Figure 2d shows a Kocks–Mecking type plot of the strain hardening rate θ ($=\frac{\partial\sigma}{\partial\varepsilon}$) vs. net flow stress ($\sigma - \sigma_y$) at a strain rate of 1×10^{-3} s^{-1}. An initial θ value of about 9,500 MPa decreased rapidly and linearly, exhibiting stage III hardening behavior in the BM. When the net flow stress exceeded ~40 MPa, θ became small and hardening stage IV occurred. The FSWed joints showed an initial higher θ value of about 10,800, 11,000, and 12,000 MPa at welding speeds of 100, 200, and 400 mm/min, respectively, and also a linear decrease but with a smaller slope in comparison to the BM (Fig. 2d). Similarly, stage III hardening appeared immediately after yielding, without the presence of stage II hardening, followed by Stage IV hardening in the FSWed joints as well. It is also seen from Fig. 2d that the net flow stress became larger after welding, and it increased with increasing welding speed.

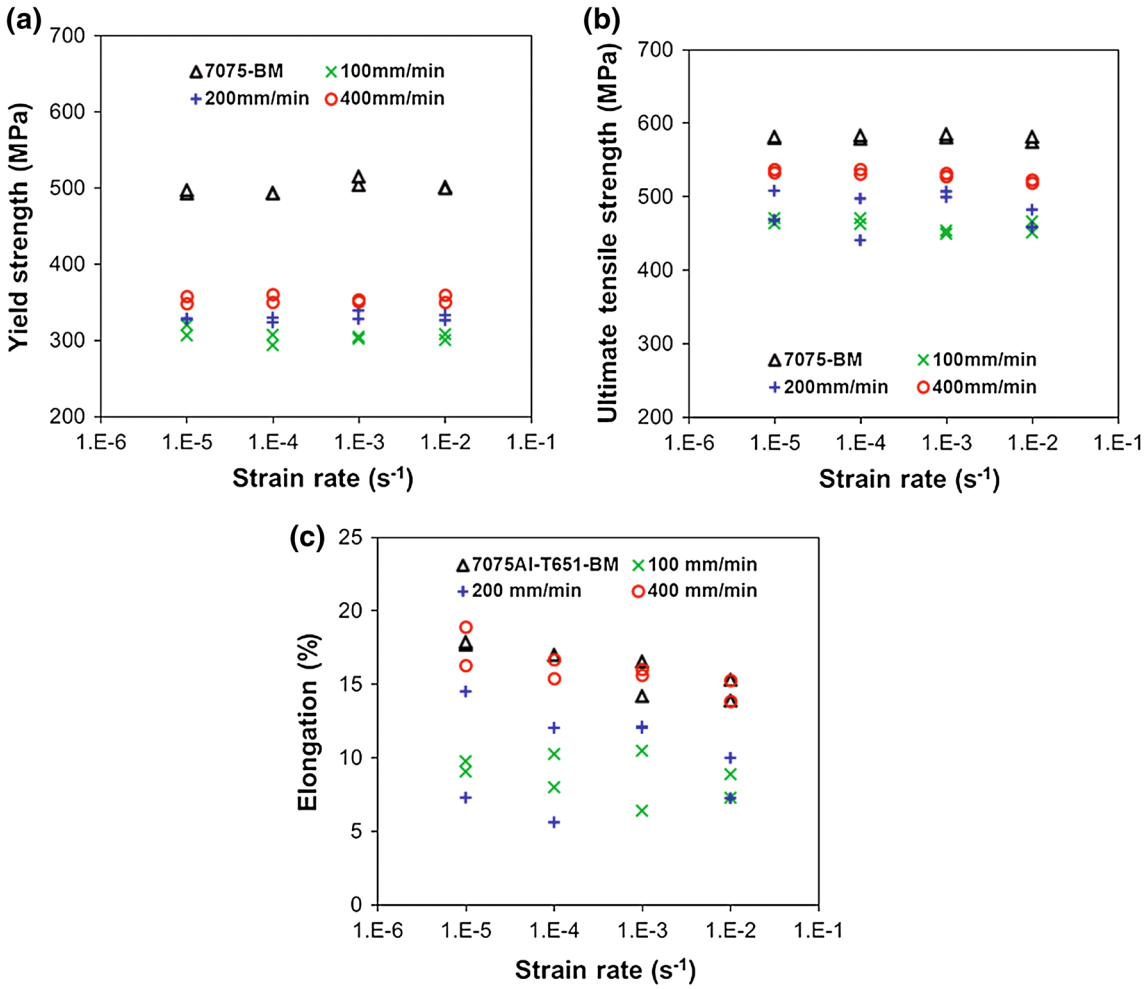

Fig. 3 Effect of strain rate on the tensile properties of FSWed 7075Al-T651 joints made with 800 r/min and tested at different strain rates: **a** YS, **b** UTS, **c** ductility

The hardening capacity, H_c, proposed by Afrin et al. [8],

$$H_c = \frac{\sigma_{UTS} - \sigma_y}{\sigma_y} = \frac{\sigma_{UTS}}{\sigma_y} - 1, \quad (4)$$

was further used to evaluate the hardening behavior of the BM and FSWed 7075Al-T651 joints (Table 1). While FSW led to a lower strength, similar to the strain hardening exponents (Fig. 2c) the hardening capacity was considerably (over 3 times) higher. To understand the strain hardening behavior, it is necessary to consider both strengthening effects of the grain sizes and dislocation interactions. A strain hardening model taking such effects into account could be expressed as [39, 40],

$$\sigma = \sigma_0 + \sigma_{HP} + \sigma_d, \quad (5)$$

where σ_0 is the frictional contribution, $\sigma_{HP} = kd^{-1/2}$ is the Hall–Petch contribution reflecting the effect of grain size d, and $\sigma_d = M\alpha Gb\rho^{1/2}$ is the Taylor dislocation contribution, ρ is the dislocation density, α is a constant, M is the Taylor factor, G is the shear modulus, and b is the Burgers vector. As the number of dislocations increased during plastic deformation, the spacing among them became smaller and their interactions were more repulsive, which ultimately increased the resistance to deformation. Based on Eq. (5), the finer the grain size was, the stronger the Hall–Petch contribution σ_{HP} was, leading to a higher initial hardening rate in the case of 400 mm/min (Fig. 2d) due to its smaller grain size (Fig. 1a). The increase of the strain hardening rate with decreasing the grain size was reported in cadmium by Risebrough and Teghtsoonian [41] due to either higher hardening rate of the nonbasal system or an increase in forest dislocation density through the motion of basal dislocations. Sinclair et al. [42] and Kovacs et al. [43] also reported that at lower strains, the grain size had a strong contribution to the strain hardening and the influence of the grain size on the strain hardening faded away at higher strains due to dislocation screening and dynamic recovery effects at the grain boundaries. The much higher hardening

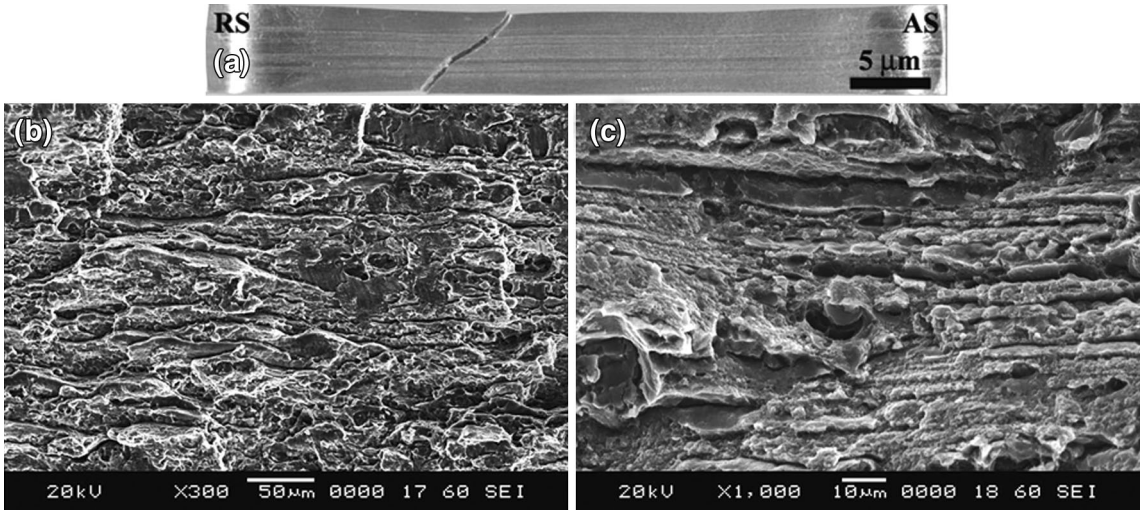

Fig. 4 A typical FSWed 7075Al-T651 joint made with 800 r/min–400 mm/min and tested at a strain rate of 1×10^{-3} s^{-1}: **a** a macroscopic image showing the failure location (AS: advancing side; RS: retreating side; and Top: welding plane), **b** SEM micrograph at a lower magnification, **c** SEM micrograph at a higher magnification

capacity after FSW (Table 1) was primarily associated with the recrystallized grains without the presence of original precipitates and with a relatively low dislocation density prior to deformation (Fig. 1). Such recrystallized grains with emptier interior spaces (free of precipitates in conjunction with fewer pre-existing dislocations) would have a stronger dislocation storage capacity as the number of dislocations increased during tensile deformation, thus giving rise to a much higher hardening capacity after FSW, as shown in Table 1.

Figure 3 shows the effect of strain rate on the tensile properties of FSWed 7075Al-T651 joints. While the %El decreased with increasing strain rate, the YS and UTS were nearly independent of the strain rate, which indicated that the strain rate sensitivity was basically absent for both the 7075Al-T651 BM and welded joints. It is also seen that while the yield strength decreased after welding (Fig. 3a), the ultimate tensile strength only modestly decreased (Fig. 3b), thus giving rise to much higher hardening capacity (Table 1). It is of particular interest to observe from Fig. 3c that there was indeed no reduction in the ductility in the case of welding speed of 400 mm/min, although it decreased in the cases of the lower welding speeds. This suggests that FSW is a robust welding technique in joining 7075Al-T651 Al alloy, *i.e.*, as long as the welding parameters were optimized, nearly the same values of both strength and ductility as those of BM could be achieved.

Figure 4 shows typical failure location and fracture surface of FSWed 7075Al-T651 alloy. The observation direction of the macroscopic image was similar with our previous work [22], in which the typical cross-sectional macrostructures and microhardness contour maps of the FSWed 7075Al-T651 joints were observed and analyzed in detail. In view of this, the failure basically occurred between the thermomechanically affected zone and heat-affected zone with an angle of $\sim 45^{o}$ to the tensile axis in the retreating side (RS). The long and flat regions on the fracture surface corresponded to the elongated grains, separated by ductile tear ridges (Fig. 4b, c). Similar results were also observed by Mahoney et al. [21]. It was reported that the tensile fracture path of the welds corresponded to the low hardness zones (LHZs) [36, 44, 45], as observed in most cases of lower welding speeds in the present study. However, in the present case of higher welding speed of 400 mm/min most samples tested at different strain rates did not fail in the LHZs, as shown in Fig. 4a. This was due to the fact that the LHZs of the sample welded at 400 mm/min were nearly absent, compared with those at 100 mm/min [22]. This would be the reason why the ductility of the samples welded at a welding speed of 400 mm/min was equivalent to that of the BM. Based on these results one could conclude that the optimal welding parameters for the high-strength 7075Al-T651 Al alloy were 800 r/min and 400 mm/min.

4 Conclusions

(1) The nugget zone of 7075Al-T651 Al alloy after friction stir welding was observed to consist of fine and equiaxed recrystallized grains with a relatively low dislocation density and free of original precipitates due to high temperatures experienced, but containing uniformly distributed dispersoids.

(2) The yield strength, ultimate tensile strength, ductility, joint efficiency, and net flow stress after yielding all increased with increasing welding speed in the FSWed joints.

(3) A joint efficiency of ~91% was achieved at a rotational rate of 800 r/min and welding speed of 400 mm/min, and in this welding condition, the ductility remained essentially the same as that of the base metal.
(4) Friction stir welding resulted in appreciably higher hardening capacity and strain hardening exponent due to a stronger dislocation storage capacity in the recrystallized grains.
(5) While both the base metal and FSWed joints exhibited stage III hardening after yielding, followed by stage IV hardening, the initial strain hardening rate was higher and the net flow stress extended further in the FSWed joints than in the base metal.
(6) While the ductility decreased with increasing strain rate, the yield strength and ultimate tensile strength were nearly independent of the strain rate, indicating the absence of strain rate sensitivity in both base metal and welded joints of the 7075Al-T651 Al alloy.

Acknowledgments This work was financially supported by Natural Sciences and Engineering Research Council of Canada (NSERC), Premier's Research Excellence Award (PREA), NSERC-DAS Award, Canada Foundation for Innovation (CFI), Ryerson Research Chair (RRC) program, National Outstanding Young Scientist Foundation of China (No. 50525103), and Hundred Talents Program of the Chinese Academy of Sciences. The authors also thank Messrs. Q. Li, A. Machin, J. Amankrah, D. Ostrom and R. Churaman for their assistance in the experiments.

References

[1] J.R. Davis, *ASM Specialty Handbook, Aluminum and Aluminum Alloys* (The Materials Information Society, 1993)
[2] W.M. Thomas, E.D. Nicholas, J.C. Needham, M.G. Murch, P. Templesmith, C.J. Dawes, GB Patent Application No. 9125978.8, December, 1991
[3] R.S. Mishra, Z.Y. Ma, Mater. Sci. Eng. R **50**, 1 (2005)
[4] R. Nandan, T. DebRoy, H.K.D.H. Bhadeshia, Prog. Mater Sci. **53**, 980 (2008)
[5] P.L. Threadgill, A.J. Leonard, H.R. Shercliff, P.J. Withers, Int. Mater. Rev. **54**, 49 (2009)
[6] G. Cam, Int. Mater. Rev. **56**, 1 (2011)
[7] A.H. Feng, Z.Y. Ma, Scr. Mater. **56**, 397 (2007)
[8] N. Afrin, D.L. Chen, X. Cao, M. Jahazi, Scr. Mater. **57**, 1004 (2007)
[9] G.M. Xie, Z.Y. Ma, L. Geng, R.S. Chen, Mater. Sci. Eng. **A471**, 63 (2007)
[10] M. Fairman, N. Afrin, D.L. Chen, X.J. Cao, M. Jahazi, Can. Metall. Q. **46**, 425 (2007)
[11] N. Afrin, D.L. Chen, X. Cao, M. Jahazi, Mater. Sci. Eng. **A472**, 179 (2008)
[12] S.M. Chowdhury, D.L. Chen, S.D. Bhole, X. Cao, E. Powidajko, D.C. Weckman, Y. Zhou, Mater. Sci. Eng. A **527**, 2951 (2010)
[13] W.B. Lee, C.Y. Lee, W.S. Chang, Y.M. Yeon, S.B. Jung, Mater. Lett. **59**, 3315 (2005)
[14] A.P. Reynolds, E. Hood, W. Tang, Scr. Mater. **52**, 491 (2005)
[15] C.G. Rhodes, M.W. Mahoney, W.H. Bingel, R.A. Spurling, C.C. Bampton, Scr. Mater. **36**, 69 (1997)
[16] J.Q. Su, T.W. Nelson, R. Mishra, M. Mahoney, Acta Mater. **51**, 713 (2003)
[17] C.G. Rhodes, M.W. Mahoney, W.H. Bingel, M. Calabrese, Scr. Mater. **48**, 1451 (2003)
[18] J. Kang, G.H. Luan, R.D. Fu, Acta Metall. Sin. **47**, 224 (2011). (in Chinese)
[19] C.B. Fuller, M.W. Mahoney, M. Calabrese, L. Micona, Mater. Sci. Eng. A **527**, 2233 (2010)
[20] K.V. Jata, K.K. Sankaran, J.J. Ruschau, Metall. Mater. Trans. **31A**, 2181 (2000)
[21] M.W. Mahoney, C.G. Rhodes, J.G. Flintoff, R.A. Spurling, W.H. Bingel, Metall. Mater. Trans. **29A**, 1955 (1998)
[22] A.H. Feng, D.L. Chen, Z.Y. Ma, Metall. Mater. Trans. **41A**, 957 (2010)
[23] C.M. Hu, C.M. Lai, P.W. Kao, N.J. Ho, J.C. Huang, Scr. Mater. **60**, 639 (2009)
[24] X.Z. Lin, D.L. Chen, J. Mater. Eng. Perform. **17**, 894 (2008)
[25] W.F. Xu, J.H. Liu, D.L. Chen, G.H. Luan, J.S. Yao, Adv. Mater. Res. **291–294**, 833 (2011)
[26] A. Simar, K.L. Nielsen, B.D. Meester, T. Pardoen, V. Tvergaard, Mater. Sci. Forum **638–642**, 333 (2010)
[27] H. Khodaverdizadeh, A. Mahmoudi, A. Heidarzadeh, E. Nazari, Mater. Des. **35**, 330 (2012)
[28] L. Commin, M. Dumont, J.E. Masse, L. Barrallier, Acta Mater. **57**, 326 (2009)
[29] V.K. Patel, S.D. Bhole, D.L. Chen, Scr. Mater. **65**, 911 (2011)
[30] T.R. McNelley, S. Swaminathan, J.Q. Su, Scr. Mater. **58**, 349 (2008)
[31] J.G. Byrne, *Recovery, Recrystallization, and Grain Growth* (Macmillan Company, New York, 1965)
[32] J.Q. Su, T.W. Nelson, C.J. Sterling, Mater. Sci. Eng. A **405**, 277 (2005)
[33] J.Q. Su, T.W. Nelson, C.J. Sterling, Philos. Mag. **86**, 1 (2006)
[34] A.M. Russell, K.L. Lee, *Structure-Property Relations in Nonferrous Metals* (Wiley, Hoboken, 2005)
[35] M. Cabibbo, E. Meccia, E. Evangelista, Mater. Chem. Phys. **81**, 289 (2003)
[36] A.H. Feng, D.L. Chen, Z.Y. Ma, Metall. Mater. Trans. **41A**, 2626 (2010)
[37] W.F. Hosford, *Mechanical Behavior of Materials* (University of Michigan, Cambridge University Press, New York, 2005)
[38] X.H. Chen, L. Lu, Scr. Mater. **57**, 133 (2007)
[39] J.A.D. Valle, F. Carreno, O.A. Ruano, Acta Mater. **54**, 4247 (2006)
[40] J.A.D. Valle, O.A. Ruano, Scr. Mater. **55**, 775 (2006)
[41] N.R. Risbrough, E. Teghtsoonian, Can. J. Phys. **45**, 591 (1967)
[42] C.W. Sinclair, W.J. Poole, Y. Bréchet, Scr. Mater. **55**, 739 (2006)
[43] I. Kovacs, N.Q. Chinh, E.K. Csetenyi, Phys. Stat. Sol. A **194**, 3 (2002)
[44] F.C. Liu, Z.Y. Ma, Metall. Mater. Trans. **39A**, 2378 (2008)
[45] A.H. Feng, D.L. Chen, Z.Y. Ma, Mater. Sci. Forum **618–619**, 41 (2009)